added, though in all cases our samples contain a concentration of free CO at least as large as the initial concentration of $Fe(CO)_5$. A thermopile detector measures attenuation of light by the reaction mixture, while product (ethane) yields are monitored at intervals by flame ionization gas chromatography.

The catalyst precursor, $Fe(CO)_4(C_2H_4)$, is prepared in situ by irradiation of $Fe(CO)_5$ in the presence of reactants.[23] This precatalyst is a stable species that does not revert to $Fe(CO)_5$ but photodecomposes to form the coordinatively unsaturated active catalyst, $Fe(CO)_3(C_2H_4)$, which promotes hydrogenation until it recombines with CO.

We find that CO added to the reaction mixture decreases the quantum yield (defined as the number of product molcules formed per photon absorbed). This decrease is systematic, yielding the inverse dependence of the quantum yield on CO pressure shown in Figure 1. The observed quantum efficiency also depends on the repetition rate of the laser, falling from a maximum value which is constant at low repetition rates to intersect the minimum quantum yield found under conditions of continuous wave illumination (see Figure 2).

The elementary behavior of the catalytic system responsible for these two observations can be understood by examining the simple kinetics of catalytic hydrogenation in competition with catalyst–CO recombination, viz.

$$Fe(CO)_3(C_2H_4) \xrightarrow[\text{TOR}]{H_2,C_2H_4} C_2H_6 + Fe(CO)_3(C_2H_4) \quad (1)$$

$$Fe(CO)_3(C_2H_4) \xrightarrow[k_R[CO]=\tau^{-1}]{CO} Fe(CO)_4(C_2H_4) \quad (2)$$

Here we associate a turnover rate (TOR) with the formation of product, and since the concentration of free CO is always large compared to that of active catalyst, we assign a pseudo-first-order rate constant, $k_R[CO]$, to the relaxation of the system back to precatalyst.

Figure 2 shows that at low repetition rates the catalytic quantum yield is maximized. Under such conditions if we can assume that every photon absorbed produces a catalyst, we can write down a simple relation between the turnover rate, the relaxation rate, and this maximum quantum yield. The turnover rate is the number of product molecules produced per catalyst divided by the average amount of time the catalyst works before its reversion, τ. Under our assumption of one catalyst formed per photon absorbed, the amount of product per catalyst is the same as the amount of product per photon, or the quantum yield, Φ_{max}. Thus

$$\text{TOR} = \Phi_{max}/\tau = \Phi_{max}k_R[CO] \quad (3)$$

As shown in Figure 1, a plot of Φ_{max}^{-1} vs. CO pressure is indeed linear, yielding by its slope the ratio $k_R/\text{TOR} = 100 \pm 1\ M^{-1}$.

At high laser-pulse repetition rates, where the time between pulses is less than τ, a given pulse irradiates both precatalyst and still-active catalyst remaining from previous pulses, and we observe our assumption of one catalyst produced per photon absorbed to fail. The quantum yield, which is constant at slow repetition rates, diminishes with closer spaced pulses. Analysis of this time-between-pulses (rep rate) dependence allows us to calculate the average lifetime of the catalyst.

We consider four processes to occur with the advent of each laser pulse: (1) photoejection of CO from precatalyst with unit quantum efficiency to create active catalyst; (2) absorption of light by catalyst remaining from previous pulses, resulting in the irreversible loss of catalytic activity (again with unit efficiency); (3) catalyst recombination with CO; and (4) catalyst-promoted hydrogenation of ethylene. Processes 3 and 4 occur thermally whenever the appropriate reactants are present. From this model we obtain a recursion relation for the concentrations of catalyst and precatalyst after each successive laser pulse, which yields a geometric series in the limit of many pulses (>50). Taking into account the consumption of photons in both precatalyst and catalyst absorption channels, we calculate the quantum yield as a function of the time between laser pulses (Δt) for a given catalyst lifetime τ and catalyst absorption probability α:[24]

$$\Phi = \Phi_{max}\frac{\alpha(1-\alpha)e^{-\Delta t/\tau} + e^{\Delta t/\tau} - 1}{e^{\Delta t/\tau} - (1-2\alpha)} \quad (4)$$

This model explains the behavior pictured in Figure 2. A two-parameter nonlinear least-squares fit of the data yields the theoretical curve shown for $\alpha = 0.42$ and $\tau = 0.045$ s. Thus from eq 3 we obtain for the present conditions $\text{TOR} = 900 \pm 70\ s^{-1}$. This intrinsic rate is a thousand times faster than the fastest known liquid-phase hydrogenation system.[25] Equation 3 also yields $k_R = 9.0 \pm 0.7 \times 10^4\ M^{-1}\ s^{-1}$, which shows by comparison with the data of Ouderkirk et al.[21] that the substitution of ethylene for CO slows recombination of the unsaturated iron carbonyl fragment with CO by about 2.5 orders of magnitude.

The difference between $Fe(CO)_3(C_2H_4)$ and $Fe(CO)_4$ is interesting. We suspect that recombination in the case of the substituted carbonyl is slowed by an activation barrier, possibly associated with a required rearrangement of the ethylene ligand.[26] Temperature-dependence experiments to test this hypothess are presently underway.

Acknowledgment. We gratefully acknowledge Koppers Company, Inc. for support of this research.

Registry No. $Fe(CO)_3(C_2H_4)$, 84520-95-6; $Fe(CO)_4(C_2H_4)$, 32799-25-0; $CH_2{=}CH_2$, 74-85-1.

(23) The presence of this species together with its mechanistic significance is established by kinetic and spectroscopic evidence (see ref 1, 5, and 17).

(24) α is the product of the photon flux, catalyst extinction coefficient, and cell path length.

(25) See, for example: Collman, J. P.; Hegedus, L. S. "Principles and Applications of Organotransition Metal Chemistry"; University Science Books: Mill Valley, CA, 1980; pp 317–318.

(26) We thank C. P. Casey for discussions on this point.

Metallophosphorus Clusters: $Ru_5(CO)_{12}(\mu_4\text{-PPh})(\mu_3\text{-}CCH_2\text{-}i\text{-Pr})(\mu_2\text{-}PPh_2)$ and $HRu_5(CO)_{10}(\mu_4\text{-PPh})_2(\mu_3\text{-PPh})(\mu_2\text{-}PPh_2)$, Face-Capped-Octahedral and Pentagonal-Bipyramidal Clusters via Stepwise Reduction of an Acetylide

Karen Kwek, Nicholas J. Taylor, and Arthur J. Carty*

Guelph-Waterloo Centre, Waterloo Campus
Chemistry Department, University of Waterloo
Waterloo, Ontario N2L 3G1, Canada

Received February 27, 1984

The incorporation of main-group atoms into the skeletal frameworks of transition-metal clusters offers new opportunities to compare the predictions of current bonding theories[1] and to improve on the degradative instability of high nuclearity, homonuclear compounds.[2] We report a new synthetic route to the interesting class of metallophosphorus clusters[3] involving sequential

(1) O'Neill, M. E.; Wade, K. In "Metal Interactions with Boron Clusters"; Grimes, R. N., Ed.; Plenum Press: New York, 1982.

(2) Chini, P.; Longoni, G.; Albano, V. G. *Adv. Organomet. Chem.* **1976**, *14*, 285.

(3) Although there has recently been a considerable upsurge in interest in μ-PR groups as stabilizing, face bridging ligands in cluster chemistry, relatively few medium-to-high nuclearity clusters incorporating PR units in the skeletal framework are known. For recent references see: (a) Lower, L. D.; Dahl, L. F. *J. Am. Chem. Soc.* **1976**, *98*, 5046. (b) Pittman, C. U., Jr.; Wileman, G. M.; Wilson, W. D.; Ryan, R. C. *Angew Chem., Int. Ed. Engl.* **1980**, *19*, 478. (c) Vahrenkamp, H.; Wucherer, E. J. *Ibid.* **1981**, *20*, 680. (d) Natarajan, K.; Zsolnai, L.; Huttner, G. *J. Organomet. Chem.* **1981**, *209*, 85. (e) Vahrenkamp. H.; Wolters, D. Organometallics **1982**, *1*, 874. (f) Kouba, J. K.; Muetterties, E. L.; Thompson, M. R.; Day, V. M. *Ibid.* **1983**, *2*, 1065. (g) Rheingold, A. L.; Sullivan, P. J. *J. Chem. Soc., Chem. Commun.* **1983**, 39. (h) Burkhardt, E. W.; Mercer, W. C.; Geoffroy, G. L.; Rheingold, A. L.; Fultz, W. C. *Ibid.* **1983**, 1251. (i) Jones, R. A.; Whittlesey, B. R. *Organometallics* **1984**, *3*, 469.

0002-7863/84/1506-4636$01.50/0

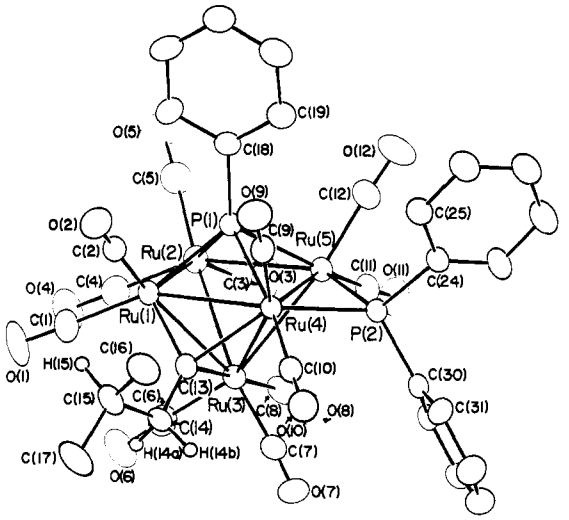

Figure 1. Structure of $Ru_5(CO)_{12}(\mu_4\text{-PPh})(\mu_3\text{-}CCH_2\text{-}i\text{-Pr})(\mu_2\text{-}PPh_2)$ (**2**) showing the capped octahedral stereochemistry of the Ru_5PC skeleton.

reduction of a hydrocarbyl with a primary phosphine, a method with considerable potential for polyhedral expansion since many clusters with multisite bound unsaturated ligands are known.[4] This general strategy and the structures of two clusters, capped-octahedral $Ru_5(CO)_{12}(\mu_4\text{-PPh})(\mu_3\text{-}CCH_2\text{-}i\text{-Pr})(\mu_2\text{-}PPh_2)$ (**2**) and capped-pentagonal-bipyramidal $HRu_5(CO)_{10}(\mu_4\text{-PPh})(\mu_3\text{-PPh})(\mu_2\text{-}PPh_2)$ (**3**), which precisely illustrate the *n*-vertex, *n*-electron pair capping principle[5] for mixed main-group–transition-metal clusters, are described herein.

Treatment of $Ru_5(CO)_{13}(\mu_4\text{-}\eta^2\text{-}C{\equiv}C\text{-}i\text{-Pr})(\mu\text{-}PPh_2)$[6] (**1**) (0.32 g, 0.28 mmol) with $PPhH_2$ (0.046 g, 0.41 mmol) in toluene (14 mL) at 107 °C for 4.5 h afforded several products separable by chromatography on Florisil (eluant *n*-hexane). Major products were a dark red band (II) which afforded red crystals of **3** (60%) on cooling at 0 °C (IR, ν(CO) (C_6H_{12}): 2047 w, 2033 w, 2019 s, 2013 s, 1972 m; deceptively simple ^{31}P NMR (C_7D_8, −70 °C): δ +362 (d) (μ-PPh); +252 (d) (μ_2-PPh_2); ^1H NMR (C_6D_6): δ 7.24 (m), C_6H_5; −16.70 (m), hydridic H) and a brown band (IV) from which red-brown crystals of **2** (20%) were obtained on crystallization in hexane/benzene (IR, ν(CO) (C_6H_{12}): 2072 m, 2054 s, 2032 s, 2020 s, 2007 s, 1981 w, 1960 w cm^{-1}; ^{31}P NMR (C_7D_8, −70 °C): δ +287 (d) (μ_4-PPh), +251.0 (d) (μ_2-PPh_2); ^1H NMR (C_6D_6): δ 7.4 (m) (C_6H_5)). Both **2** and **3** were characterized by single-crystal X-ray diffraction.[7] The structure of **2** (Figure 1) consists of an octahedron of five ruthenium atoms and a phosphorus atom with one face (Ru(1)–Ru(3)–Ru(4)) capped by the carbon atom C(13) of an alkylidyne (CCH_2-*i*-Pr) group. The phosphido (PPh_2) bridged square-pyramidal metal skeleton of **2** bears a close structural resemblance to the precursor **1**.[6] Reduction of the μ_4-C≡C-*i*-Pr group in **1** by hydrogen transfer from $PPhH_2$ has afforded μ_4-PPh and μ_3-CCH_2-*i*-Pr groups with the former ligand in the capping site previously occupied by C_α of the acetylide.

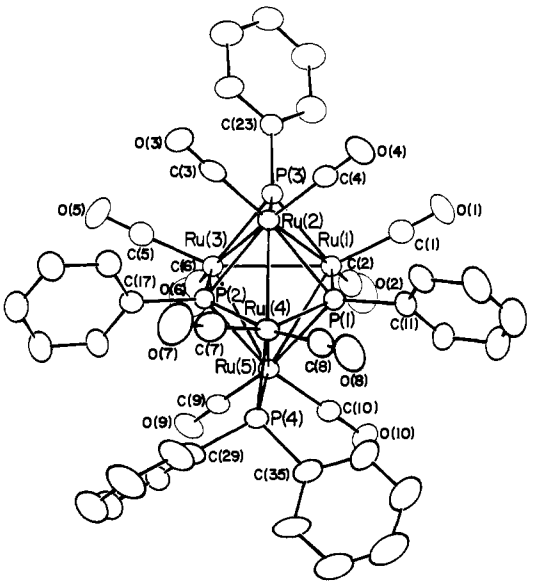

Figure 2. ORTEP drawing of the structure of $HRu_5(CO)_{10}(\mu_4\text{-PPh})_2(\mu_3\text{-PPh})(\mu_2\text{-}PPh_2)\cdot 0.5C_6H_6$ with the solvent of crystallization not shown. The hydrogen atom is located on the Ru(1)–Ru(3)–Ru(5) face.

Scheme I

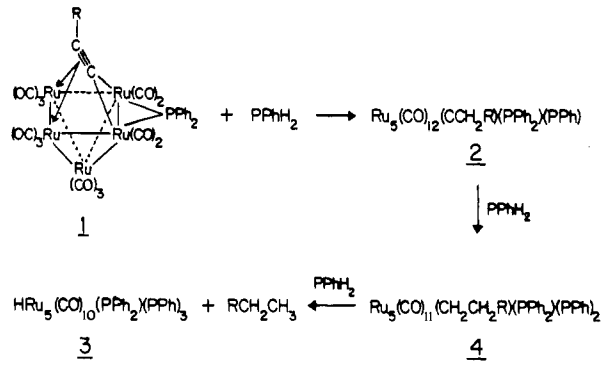

Examples of acetylide reduction to an alkylidyne are rare.[8] The alkylidyne ligand is unsymmetrically coordinated, with two Ru–C bond lengths [Ru(1)–C(13) 2.174 (5), Ru(4)–C(13) 2.199 (4) Å] longer than the third [Ru(1)–C(13) 1.917 (5) Å]. In **3** (Figure 2) five ruthenium atoms and the three phenylphosphinidenes make up a face-capped pentagonal-bipyramidal skeleton. Two of the PPh groups occupy equatorial positions with the third capping the Ru(1)–Ru(2)–Ru(3) face; P(4) bridges the Ru(4)–Ru(5) edge as a μ-PPh_2 group. Examination of Ru–Ru–C(0) bond angles and the coordination surface of the cluster strongly suggested a μ_3-bonding mode for the hydride on the Ru(1)–Ru(3)–Ru(5) face.[9] Although μ_2-PPh_2, μ_3-PPh, and μ_4-PPh groups are well-known in cluster chemistry,[3] the presence of all three types in a cluster is unusual.

A plausible scheme for the stepwise conversion **1** → **3** (Scheme I) involves the intermediacy of **2** and an unstable alkyl complex **4** which has not been isolated. In agreement with this mechanism, treatment of isolated **2** with 2 molar equiv. of $PhPH_2$ in toluene at 25 °C affords **3** quantitatively.

The capped geometries of **2** and **3** pose an interesting test of current bonding descriptions for clusters. Consideration of the μ-PPh group as contributing four electrons for framework bonding leads to a skeletal electron count of eight pairs for **3**, appropriate for a 7-vertex closo polyhedron. Accordingly one skeletal atom would be expected to occupy a face capping position, as is observed.

(4) Sappa, E.; Tiripicchio, A.; Braunstein, P. *Chem. Rev.* **1983**, *83*, 203.
(5) Wade, K. *Adv. Inorg. Chem. Radiochem.* **1976**, *18*, 1. See also: Mingos, D. M. P. *J. Chem. Soc., Chem. Commun.* **1983**, 706.
(6) (a) Carty, A. J.; Taylor, N. J.; MacLaughlin, S. A. *J. Am. Chem. Soc.* **1981**, *103*, 2456. (b) MacLaughlin, S. A.; Taylor, N. J.; Carty, A. J. *Organometallics* **1983**, *2*, 1194.
(7) Crystal data for $Ru_5P_2O_{12}C_{35}H_{24}$ (**2**): M_r 1203.87, monoclinic, space group $P2_1/c$, a = 11.724 (1) Å, b = 16.752 (2) Å, c = 20.617 (2) Å, β = 94.05 (1)°, Z = 4, ρ_m = 1.96, ρ_c = 1.980 g cm^{-3}, μ(Mo Kα) = 19.20 cm^{-1}. The structure was solved and refined by using 4309 observed ($I \geq 3\sigma(I)$) (5311 measured) reflections on a Syntex $P2_1$ diffractometer to R and R_w values of 0.023 and 0.027. Crystal data for $Ru_5P_4O_{10}C_{43}H_{29}$ (**3**): M_r 1334.95, monoclinic, space group $P2_1/n$, a = 9.909 (1) Å, b = 23.004 (4) Å, c = 21.124 (3) Å, β = 102.07 (1)°, Z = 4, ρ_m = 1.87, ρ_c = 1.883 g cm^{-3}, μ(Mo Kα) = 17.18 cm^{-1}. A total of 4491 observed (6187 measured) reflections were used to solve and refine the structure to R and R_w values of 0.033 and 0.037, respectively. Further details of data collection, reduction, and refinement are given in Supplementary Table I.
(8) Castiglioni, M.; Gervasio, G.; Sappa, E. *Inorg. Chim. Acta.* **1981**, *49*, 217.
(9) Although the hydride was located in a difference Fourier synthesis, it did not behave well on refinement and was not included in subsequent calculations. A hydride signal at −16.70 ppm in the ^1H NMR confirmed its presence.

For **2** the seven skeletal pairs are appropriate for a capped closo 6-vertex polyhedron. Thus the geometries of both **2** and **3** are consistent with the *n*-bond pair, capped $n - 1$ vertex principle of SEC theory.[5] Very few examples of 7-pair, capped octahedral clusters are known. They include $Os_7(CO)_{21}$,[10] $[Rh_7(CO)_{16}]^{3-}$,[11] $[Rh_7(CO)_{16}I]^{2-}$,[12] and the cobaltaborane $[1,2,3\text{-}\{Co(\eta^5\text{-}C_5H_5)\}_3\text{-}(B_4H_4)]$.[13] The capped-pentagonal-bipyramidal polyhedron of **3** appears to be the first documented example of this geometry for an 8-vertex, 8-skeletal pair system and is particularly notable since it has been shown[14] that the dodecahedral structure, exemplified by $(\eta^5\text{-}C_5H_5)_4Co_4B_4H_4$,[15] may also accommodate this electron count. Finally we note the isolobal relationships[16] Ph–P ↔ CH^- and $M(CO)_2$ (M = Fe, Ru, Os) ↔ CH^{3+}. Thus entire series of *closo*-$M_x(CO)_{2x+1}(PPh)_x$, *nido*-$M_x(CO)_{2x+2}(PPh)_x$, or capped $n - 1$ vertex ($n = 2x$) $M_x(CO)_{2x}(PPh)_x$ metallophosphorus clusters should exist. We are currently exploring these possibilities.

Acknowledgment. This work was supported by the Natural Sciences and Engineering Research Council of Canada.

Registry No. 1, 90696-73-4; **2**, 90696-74-5; **3**, 90696-75-6; **3**·0.5C_6H_6, 90696-76-7; $PPhH_2$, 638-21-1; Ru, 7440-18-8.

Supplementary Material Available: X-ray data, collection, reduction, and refinement (Table I), lists of atomic coordinates (Tables II and V), thermal parameters (Tables III and VI), and bond lengths and angles (Tables IV and VII) for **2** and **3**, respectively (18 pages). Ordering information is given on any current masthead page. Structure factor tables for **2** and **3** are available on request from the authors.

(10) Eady, C. R.; Johnson, B. F. G.; Lewis, J.; Mason, R.; Hitchcock, P. B.; Thomas, K. M. *J. Chem. Soc., Chem. Commun.* **1977**, 385. The anion $Os_8(CO)_{22}^{2-}$ with 7 skeletal pairs has a bicapped octahedral structure. See: Jackson, P. F.; Johnson, B. F. G.; Lewis, J.; Raithby, P. R. *J. Chem. Soc., Chem. Commun.* **1980**, 60.
(11) Albano, V. G.; Bellon, P. L.; Ciani, G. F. *J. Chem. Soc., Chem. Commun.* **1969**, 1024.
(12) Albano, V. G.; Ciani, G.; Martinengo, S.; Chini, P.; Giordano, G. *J. Organomet. Chem.* **1975**, *88*, 381.
(13) Pipal, J. R.; Grimes, R. N. *Inorg. Chem.* **1977**, *16*, 3255.
(14) O'Neill, M. E.; Wade, K. *Inorg. Chem.* **1982**, *21*, 461.
(15) Pipal, J. R.; Grimes, R. N. *Inorg. Chem.* **1979**, *18*, 257.
(16) Hoffmann, R. *Angew. Chem., Int. Ed. Engl.* **1982**, *21*, 711.

Electron Exchange in Models for Heme Proteins

Dabney White Dixon,* Michael Barbush, and Ataollah Shirazi

Department of Chemistry, Washington University St. Louis, Missouri 63130

Received September 19, 1983

Electron transfer between two cytochromes is generally postulated to take place only through the exposed heme edge.[1] If this is the case, the protein serves as an insulator. The rate of transfer then depends upon the rate constant for diffusion of the protein, k_D, the percentage of the surface area of the protein that is occupied by the heme, ϕ, and the probability that the hemes, once in contact, will transfer an electron, $P = k_r/k_d$, where k_r is the rate constant for electron exchange between two free hemes and k_d is the rate constant for diffusion of the free heme.[2] Since $k_D \simeq k_d$

$$k = (k_r/k_d)k_D\phi^n = k_r\phi^n \qquad (1)$$

In the simplest model $n = 2$, but Sommer et al. have presented arguments that $1.5 \leq n \leq 2$.[3] In view of the fact that the heme exposure is ~1%,[4] one would expect a self-exchange rate 10^{-3} to 10^{-4} that of free heme.

Rate constants for electron self-exchange have been calculated for a few hemes from experiments involving stopped-flow cross reactions with other inorganic reagents. There is a wide spread of values:[5] $FeTPPS(H_2O)^{3-/4-}$, $\sim 1 \times 10^3$;[6] $FePPIX(H_2O)^{1-/0}$, $\sim 7 \times 10^5$;[7] $FeTMPyP(H_2O)^{5+/4+}$, 1.2×10^6; $FeTMPyP(Im)_2^{5+/4+}$, $>1 \times 10^7$; $FeTMPyP(H_2O)(OH)^{4+/3+}$, $>1 \times 10^9$;[8] and $FePPIX(CN)_2^{3-/4-}$, 8×10^{10} M^{-1} s^{-1}.[7a] The charge and spin-state effects and problems in calculating self-exchange rate constants from cross reactions with $SO_2^{-}\cdot$ make it difficult to compare these rate constants for the models with those found for heme proteins.

We have therefore determined the rate constants for electron self-exchange in free hemes from NMR line-broadening measurements[9] on mixtures of the Fe(II) and Fe(III) species. This

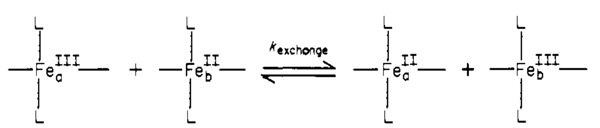

technique allows us to measure a direct self-exchange rate (no driving force for the reaction) and to use nonaqueous solvents (and therefore neutral, rather than highly charged, hemes). The Fe(II)/Fe(III) mixtures are in the fast-exchange limit. Tetraphenylporphyrin derivatives have been used because they have less tendency to aggregate and fewer resonances than the natural hemes.[10]

Table I. Electron Self-Exchange Rate Constants in Model Hemes[a]

complex	$10^{-7}k$, M^{-1} s^{-1}
$FeTPP(1\text{-}MeIm)_2$	8.1 ± 0.7
$Fe(3\text{-}MeTPP)(1\text{-}MeIm)_2$	5.3 ± 0.6
$Fe(4\text{-}MeTPP)(1\text{-}MeIm)_2$	9.7 ± 0.8
$Fe(4\text{-}OMeTPP)(1\text{-}MeIm)_2$	6.8 ± 0.6

[a] Measured in CD_2Cl_2 at −21 °C.

The electron self-exchange rates of bis-1-MeIm hemes were measured in CD_2Cl_2. It was necessary to cool the solutions to −21 °C to prevent broadening of the peaks due to ligand exchange. Under these conditions the lifetime of the six-coordinate species is ~9 s for $Fe(III)TPP(1\text{-}MeIm)_2^+Cl^-$ (ref 11) and >20 s for $Fe(II)TPP(1\text{-}MeIm)_2$.[12] The Fe(III) hemes were reduced to Fe(II)/Fe(III) mixtures with aqueous $Na_2S_2O_4$. The rate constants were independent of concentration in the range experimentally accessible (3–12 mM), and also independent of the extent of reduction (2–40%). Steric and electronic changes on the porphyrin periphery (3-Me, 4-Me, 4-OMe) made little difference in the rate constant (Table I).

Electron self-exchange rate constants in proteins span a wide range, from ~10^2 to ~10^7 M^{-1} s^{-1}.[13-17] In general long cyto-

(1) (a) Dickerson, R. E.; Timkovich, R. In "The Enzymes"; Boyer, P. D., Ed.; Academic Press: New York, 1975; Vol. 11, pp 397–547. (b) Salemme, F. R. *Annu. Rev. Biochem.* **1977**, *46*, 299–329. (c) Ferguson-Miller, S.; Brautigan, D. L.; Margoliash, E. In "The Porphyrins"; Dolphin D., Ed.; Academic Press: New York, 1979; Vol. 7, pp 149–240. (d) Timkovich, R. in ref 1c, pp 241–294. (e) Cusanovich, M. A. In "Bioorganic Chemistry"; van Tamelen, E. E., Ed.; Academic Press: New York, 1978; Vol. 4, pp 117–145. (f) Kraut, J. *Biochem. Soc. Trans.* **1981**, *9*, 197–202. (g) Capaldi, R. A.; Darley-Usmar, V.; Fuller, S.; Millett, F. *FEBS Lett.* **1982**, *138*, 1–7. (h) Meyer, T. E.; Kamen, M. D. *Adv. Protein Chem.* **1982**, *35*, 105–212.
(2) Sutin, N. *Adv. Chem. Ser.* **1977**, *162*, 156–172.
(3) Sommer, J.; Jonah, C.; Fukuda, R.; Bersohn, R. *J. Mol. Biol.* **1982**, *159*, 721–744.
(4) Stellwagen, E. *Nature (London)* **1978**, *275*, 73–74.
(5) Abbreviations: PPIX, protoporphyrin IX; TMPyP, tetrakis(4-*N*-methylpyridyl)porphyrin; TPPS, porphinetetrakis(4-benzenesulfonate).
(6) Chapman, R. D.; Fleischer, E. B. *J. Am. Chem. Soc.* **1982**, *104*, 1575–1582.
(7) (a) Worthington, P.; Hambright, P. *J. Inorg. Nucl. Chem.* **1980**, *42*, 1651–1654. (b) Cassatt, J. C.; Kukuruzinska, M.; Bender, J. W. *Inorg. Chem.* **1977**, *16*, 3371–3372.
(8) Pasternack, R. F.; Spiro, E. G. *J. Am. Chem. Soc.* **1978**, *100*, 968–972.
(9) Chan, M.-S.; Wahl, A. C. *J. Phys. Chem.* **1978**, *82*, 2542–2549.
(10) A study of electron self-exchange in biscyano hemes has shown that the synthetic and the natural iron porphyrins have similar rate constants. Dixon, D. W.; Shirazi, A.; Barbush, M., unpublished results.
(11) Satterlee, J. D.; La Mar, G. N.; Bold, T. J. *J. Am. Chem. Soc.* **1977**, *99*, 1088–1093.
(12) Dixon, D. W.; Barbush, M., unpublished results.

